



# IJRASET

International Journal For Research in  
Applied Science and Engineering Technology



# INTERNATIONAL JOURNAL FOR RESEARCH

IN APPLIED SCIENCE & ENGINEERING TECHNOLOGY

**Volume: 3**

**Issue: IV**

**Month of publication: April 2015**

**DOI:**

[www.ijraset.com](http://www.ijraset.com)

Call:  08813907089

E-mail ID: [ijraset@gmail.com](mailto:ijraset@gmail.com)

# Object Shadow Detection and Removal from Remotely Sensed Images

Atul A. Kolge<sup>1</sup>, Yogita K. Dubey<sup>2</sup>

<sup>1</sup>M.Tech Student (Dept. Of E&TC), YCCE Nagpur, India

<sup>2</sup>Prof. (Dept. Of E&TC), YCCE Nagpur, India

**Abstract**— In accordance with the characteristics of urban high-resolution color remote sensing images, we put forward an object shadow detection and removal method from remotely sensed images. In object shadow detection method, during image segmentation, shadow features are taken into consideration and after that using statistical feature of the images, suspected shadows are extracted. In our method, first color image is converted to gray image, after that global thresholding process is performed to detect the suspected shadow region. Next to that morphology erosion process is performed, then convolution filtering to elimination of false shadow and finally obtain coarse-shadow map, to classify the input color image into the candidate shadow pixels and the nonshadow pixels. After shadow detection, removal method used to remove shadow region to enhance the shadow images. Finally obtain recovered image. Experiments show that the new method can accurately detect shadows and remove from urban remote sensing images.

**Keywords**— Color aerial images, convolution filtering, Morphology erosion, Adaptive histogram equalization, Image adjustment, Shadow detection.

## I. INTRODUCTION

There are various high spatial resolution satellites like Resource 3, Quick Bird, IKONOS, and GeoEye for the observation of Earth and the speedy development of aerial platforms like unmanned aerial vehicles and airships. In urban areas, surface features are more complex, with a variety of objects and shadows formed by elevated objects such as high buildings, bridges, and trees. This shadow may cause faulty results in the change detection, object classification, image fusion. Detection of shadow is very important in the applications of urban remote sensing images like object recognition, image fusion, object classification and change detection. It is an important research issue to detect shadows for urban aerial images and remove it [1]. To detect shadows of color aerial images, Polidorio et al. [9] considered two properties of shadows, first is highly saturated blue/violet wavelength and second is low luminance.

Using this two shadow properties, the red, green, and blue (RGB) color aerial image is first transformed into the hue, saturation, and intensity (HSI) color model, after that segmentation process is applied to the saturation component and the intensity component to identify shadows [4],[7]. Later, Huang et al. [10] observed that the pixels in a shadow region have large hue value, low blue color value and small difference between green and blue color values. Using this observation, three experimental thresholds are determined to detect shadows in the HSI color image or model [8]. After that Tsai [2] presented an efficient algorithm to detect shadows for color aerial images. The input image can be first transformed into the hue, saturation, and intensity (HSI); hue, saturation, and value (HSV); luma, blue-difference chroma, and red-difference chroma (Y CbCr); hue, chroma, and value (HCV); or luminance, hue, and saturation (YIQ) color models [5-6]. After transformation of invariant color model, Tsai construct the ratio map by calculated the ratio of the hue over the intensity for each pixel and after then global threshold (otsu's method) of the constructed ratio map is determined to identify shadows. Experimental results show that Tsai's algorithm has better shadow detection accuracy when compared to the previous works. Also among these invariant color models, Tsai's algorithm has the best shadow detection performance for the HSI color model. In this paper, a new analysis (algorithm) method is given to detect shadows for color aerial images. First RGB color aerial image is transform to gray image and then applies a global thresholding process using Otsu's method to create a coarse-shadow map which is used for classifying the input color aerial image into the candidate shadow pixels and the non-shadow pixels. In shadow removal method, select only shadow region and then apply adaptive histogram equalization and image adjustment to enhance contrast of shadow regions. Then apply patch inpainting to obtain proper recovered original image. Under testing images, experimental results show that, the shadow detection accuracy of our new analysis (algorithm) method has better shadow detection accuracy when compared with the Tsai's (algorithm) method.

In Section II, we survey Tsai's shadow detection (algorithm) method. In Section III, our (algorithm) method is presented. Section IV, Shadow removal algorithm and in Section V, performance comparison between our proposed algorithm and Tsai's algorithm. Section VI, over all conclusions for this paper.

## International Journal for Research in Applied Science & Engineering Technology (IJRASET)

### II. PAST SHADOW DETECTION WORK BY TSAI

In this section, we survey the method (algorithm) proposed by Tsai [2]. The flowchart of Tsai’s (algorithm) method is shown in Fig.1. To detect shadows in the color aerial image, Tsai algorithm first transforms the input *RGB* image into an invariant color image or model, i.e. *HSI*, *HCV*, *HSV*, *YIQ*, or *YCbCr* color models. For each pixel, the ratio of the hue over the intensity is obtained to determine whether the pixel is a shadow pixel or not. Among these invariant color models, Tsai’s algorithm has the best shadow detection performance for the *HSI* model or image.

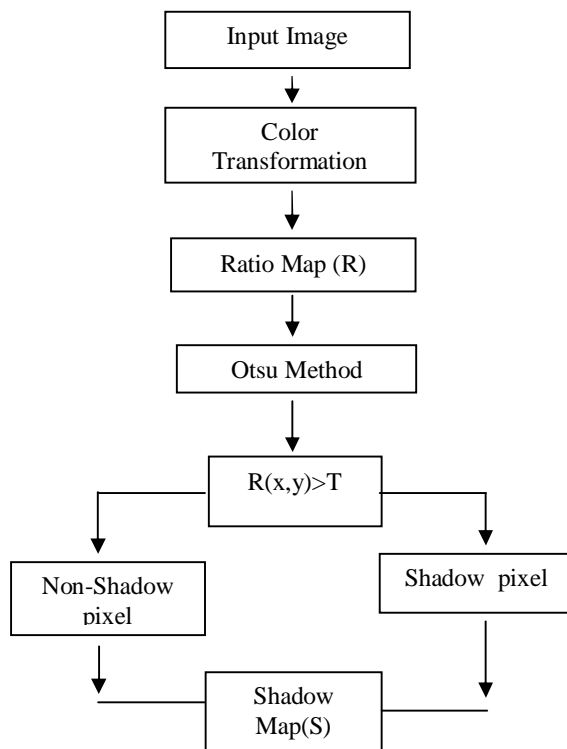


Fig.1-Tsai’s algorithm flowchart

The following equations transform the *RGB* color model into the *HSI* color model or image:

$$\begin{bmatrix} I \\ V1 \\ V2 \end{bmatrix} = \begin{bmatrix} \frac{1}{3} & \frac{1}{3} & \frac{1}{3} \\ -\sqrt{6} & -\sqrt{6} & -\sqrt{6} \\ \frac{1}{6} & \frac{1}{6} & \frac{1}{3} \\ \frac{1}{\sqrt{6}} & \frac{-2}{\sqrt{6}} & 0 \end{bmatrix} \begin{bmatrix} R \\ G \\ B \end{bmatrix}$$

$$H = \begin{cases} \tan^{-1}\left(\frac{V_2}{V_1}\right) & \text{if } V_1 \neq 1 \\ H \text{ is undefined} & \text{otherwise} \end{cases}$$

In the *HSI* model, *H* components called intensity, *I* components called hue-equivalent and *S* components called saturation. by scaling *I* and *H* components to the range in [0, 1], we can obtain the intensity-equivalent image  $I_e$  and hue-equivalent image  $H_e$ , respectively. The ratio map *R* is obtain by

$$R(x, y) = \frac{H_e(x, y) + 1}{I_e(x, y) + 1}$$

Where  $R(x, y)$ ,  $H_e(x, y)$  and  $I_e(x, y)$  denote the pixel at position  $(x, y)$  of *R*, the image  $H_e$ , and the image  $I_e$ , respectively. In Tsai’s algorithm, the value of  $R(x, y)$  is scaled to the range [0, 255] for shadow detection. Then Otsu’s thresholding method is applied on ratio map *R* to calculate the threshold *T* which can be used for separating all the pixels of *R* into two classes. Based on threshold *T*, a shadow map *S* can be obtained by

$$S(x, y) = \begin{cases} 1, & R(x, y) > T \\ 0, & \text{Otherwise} \end{cases}$$

## International Journal for Research in Applied Science & Engineering Technology (IJRASET)

### III. OUR SHADOW DETECTION ALGORITHM

In this section, our new analysis (algorithm) method is presented to detect shadows for color aerial images. The flowchart of our new analysis (algorithm) method is shown in Fig.2. We first transform RGB color image into the gray image and then, global thresholding (Otsu's method) is used to determine a global threshold T for gray image to constructing the coarse-shadow map. Next to that morphology erosion operator with  $5 \times 5$  square structuring elements is applied.

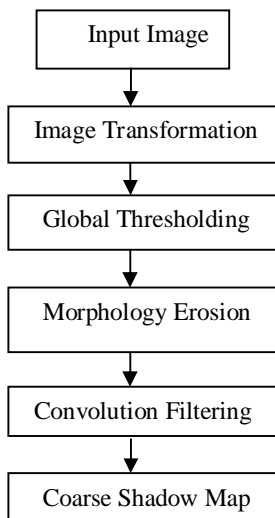


Fig.2- our new analysis based algorithm flowchart.

After that convolution filter is applied to remove noise effect and edge detection without blurring the boundaries between candidate shadow regions and nonshadow regions.

### IV. SHADOW REMOVAL ALGORITHM

In this section, Shadow removal (algorithm) method is presented to remove shadow which is detected by our new shadow detection method. Shadow removal flowchart shown in figure 3. In that shadow map is obtained from shadow detection method and input image is taken. After that selection of shadow region to obtain only shadow image. Applying adaptive histogram equalization and image adjustment on only shadow image to enhance the contrast of image. Next to patch inpainting apply to finally get enhanced shadow image.

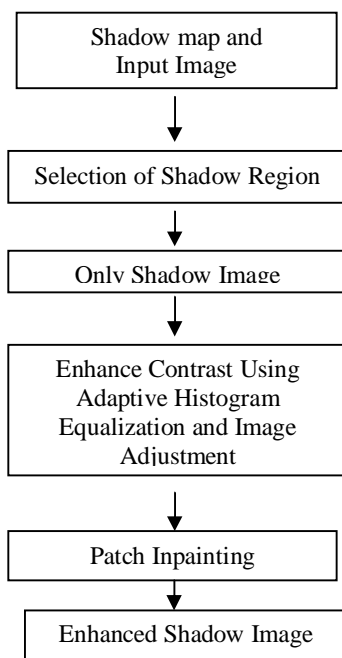


Figure 3- Shadow removal flowchart

## International Journal for Research in Applied Science & Engineering Technology (IJRASET)

### V. EXPERIMENTAL RESULTS

In this section, some experimental results are demonstrated to show the shadow detection accuracy comparison between Tsai's algorithm and our new analysis algorithm along with shadow removal. All algorithms for shadow detection and removal are executed using MATLAB.

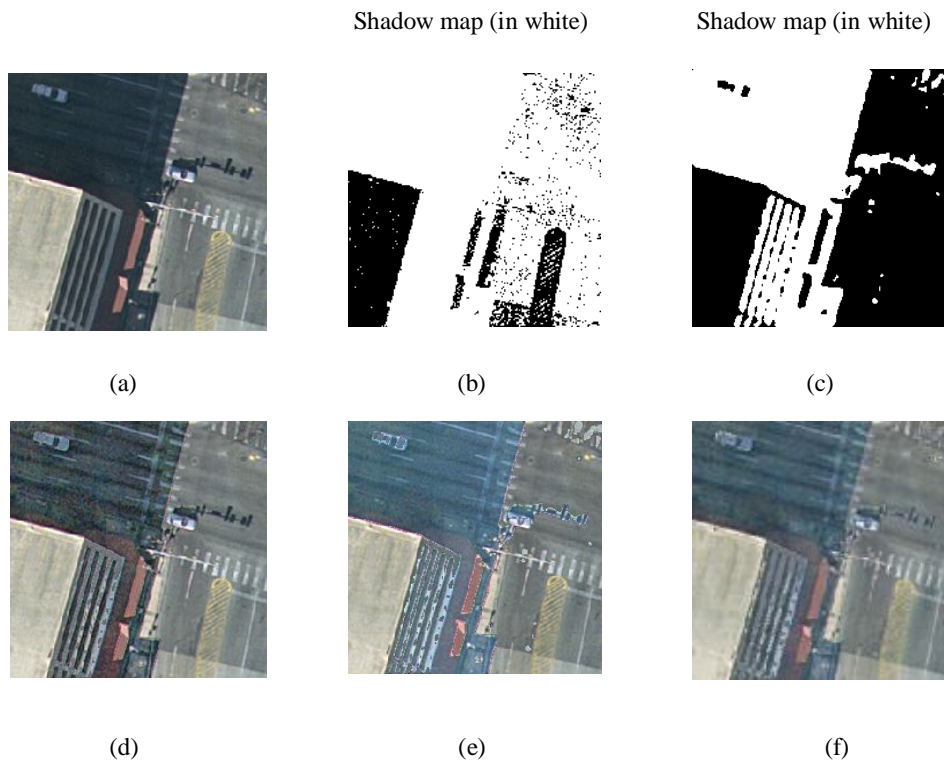
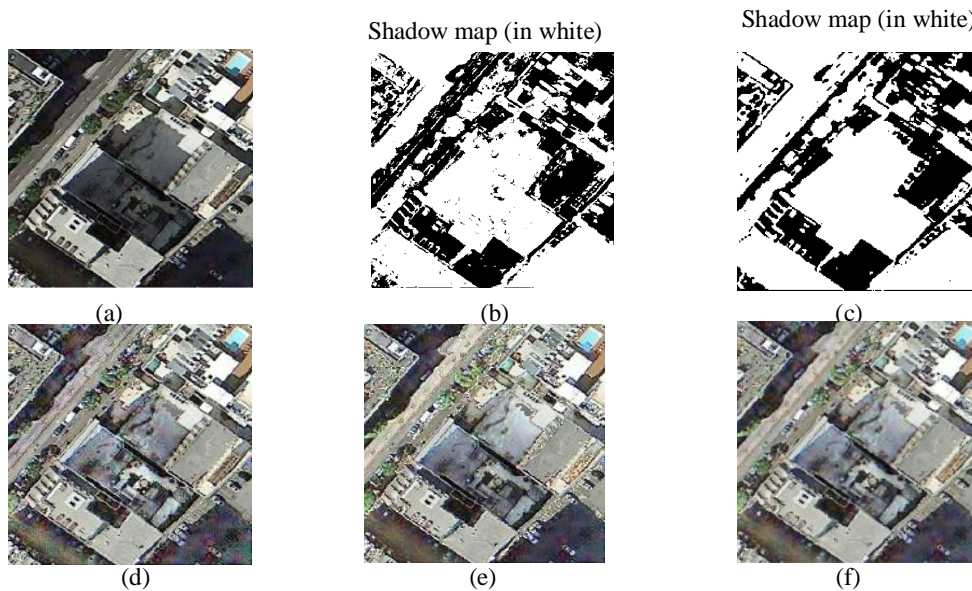


Figure 4-(a) Original image.(b) Shadow detection by Tsai's algorithm. (c) Shadow detection by our new analysis based algorithm.(d) shadow removal(Enhanced shadow image) using adaptive histogram equalization.(e) shadow removal(Enhanced shadow image) using image adjustment.(f) final shadow removal for image(a).

In Figure 4-(a) Show original image, in which shadow is formed on road due to high building on roadside and car in shadow not visible clearly. Shadow detection by tsai's algorithm shown in Figure 4(b).In that white portion nothing but shadow regions and dark portion is non-shadow regions. Shadow detection by our new analysis based algorithm shown in Figure 4(c).In which white portion is shadow regions and dark portion is non-shadow regions. Image enhancement using adaptive histogram equalization and image adjustment shown in Figure 4(d), 4(e), respectively. Final shadow removal for original image (a) shown in Figure 4(f).



## International Journal for Research in Applied Science & Engineering Technology (IJRASET)

Figure 5-(a) Original image.(b) Shadow detection by Tsai's algorithm. (c) Shadow detection by our new analysis based algorithm.(d) shadow removal(Enhanced shadow image) using adaptive histogram equalization.(e) shadow removal(Enhanced shadow image) using image adjustment.(f) final shadow removal for image(a).

In Figure 5-(a) Show original image. In which shadow on road due to high building on roadside. Shadow detection by tsai's algorithm shown in Figure 5(b).In that white portion nothing but shadow regions and dark portion is non-shadow regions. Shadow detection by our new analysis based algorithm shown in Figure 5(c).In which white portion is shadow regions and dark portion is non-shadow regions. Image enhancement using adaptive histogram equalization and image adjustment shown in Figure 5(d), 5(e), respectively. Final shadow removal for original image (a) shown in Figure 5(f). In Figure 5(f) shown that shadow remove and obtain enhanced image, and it improve quality of image.

### A. Subjective Evaluation

Figure 6(a)-10(a) show the five testing images, and the corresponding manually interpreted shadow maps, which are used as the ideal shadow maps to evaluate the shadow detection performance, are shown in Figure 6(b)-10(b), respectively. The shadow detection results of the algorithm of Tsai's algorithm and our proposed algorithm are demonstrated in Figure6(c)-10(c), and Figure6 (d)-10(d), respectively.

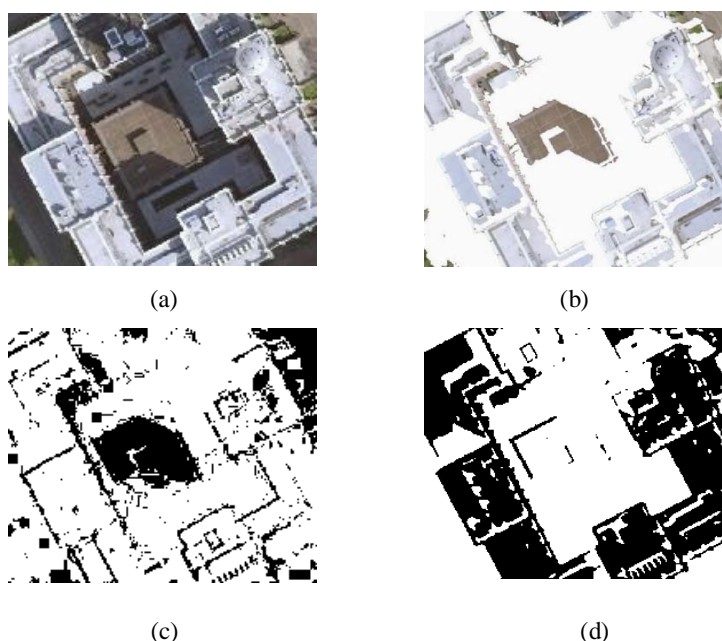


Figure6-(a) Original image. (b) Ideal shadow map. (c) Shadow detection using Tsai's algorithm. (d)Shadow detection using our based algorithm.

Original image shown in Figure 6(a). Manually interpreted shadow maps, which are used as the ideal shadow maps to evaluate the shadow detection performance, are shown in Figure 6(b).Shadow detection by Tsai's algorithm shown in Figure 6 (c) and Shadow detection by Our algorithm shown in Figure 6(d).



## International Journal for Research in Applied Science & Engineering Technology (IJRASET)

Figure7-(a) Original image. (b) Ideal shadow map. (c) Shadow detection using Tsai's algorithm.  
(d)Shadow detection using our based algorithm.

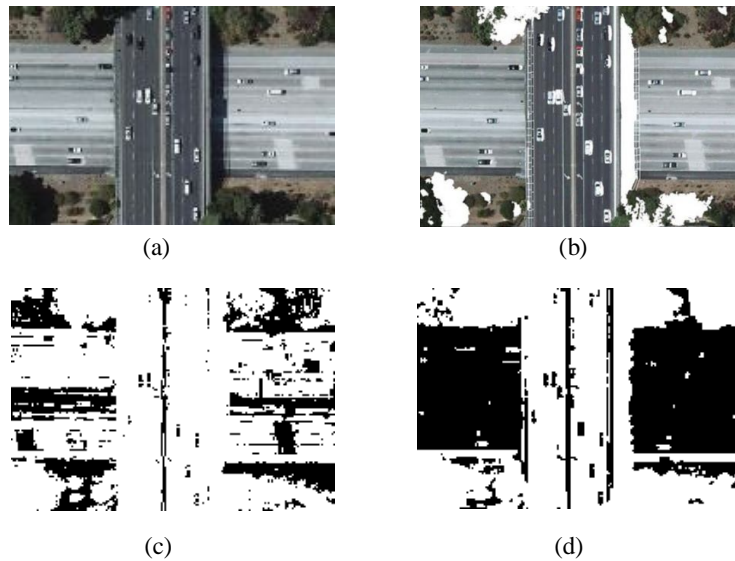


Figure8-(a) Original image. (b) Ideal shadow map. (c) Shadow detection using Tsai's algorithm.  
(d)Shadow detection using our based algorithm.

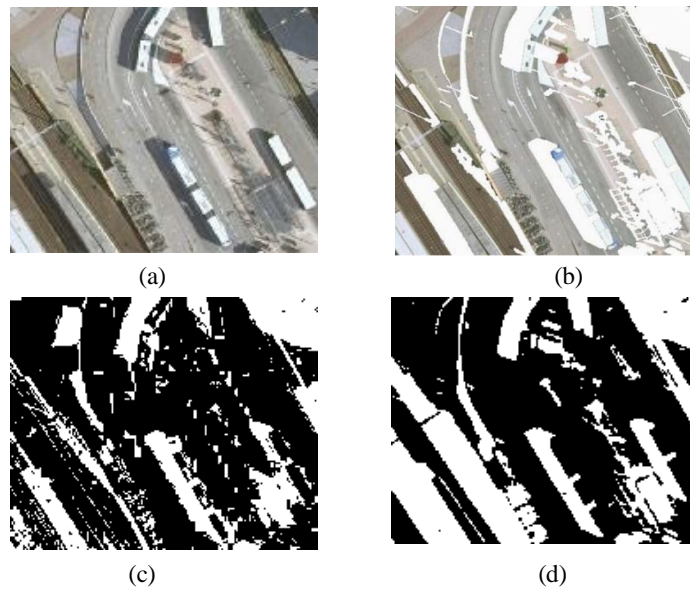
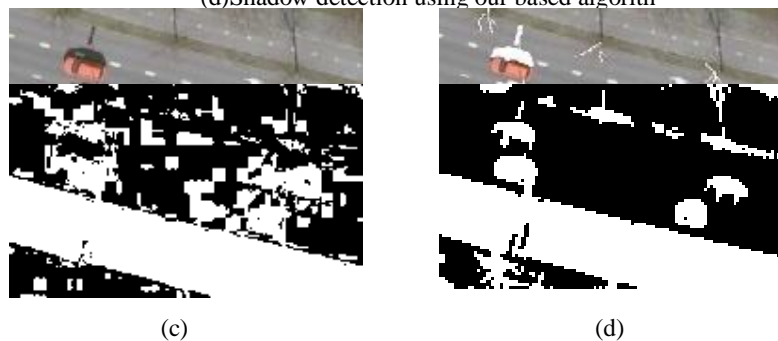


Figure9-(a) Original image. (b) Ideal shadow map. (c) Shadow detection using Tsai's algorithm.  
(d)Shadow detection using our based algorithm



## International Journal for Research in Applied Science & Engineering Technology (IJRASET)

Figure10-(a) Original image. (b) Ideal shadow map. (c) Shadow detection using Tsai’s algorithm.

(d)Shadow detection using our based algorithm

In five testing images as shown in Figure 6(a)-10(a), it is observed that our proposed algorithm has the best accuracy performance than Tsai’s algorithm and the detection results by our proposed algorithm are close to the ideal shadows marked in Figure 6(b)-10(b), respectively.

### B. Objective Evaluation

In this section, three types of accuracy, namely the producer’s accuracy, the user’s accuracy, and the overall accuracy for Tsai’s and our algorithm are used in the objective evaluation. The three types of accuracy are described as follows. The first type of accuracy is the producer’s accuracy, which contains two parameters  $\eta_s$  and  $\eta_n$ , and they are defined by

$$\eta_s = TP / (TP + FN)$$

$$\eta_n = TN / (FP + TN)$$

where true positive (TP) denotes the number of true shadow pixels which are identified correctly; false negative (FN) denotes the number of true shadow pixels which are identified as nonshadow pixels; false positive (FP) denotes the number of nonshadow pixels which are identified as true shadow pixels; and true negative (TN) is the number of nonshadow pixels which are identified correctly. The parameter  $\eta_s$  ( $\eta_n$ ) denotes the ratio of the number of correctly detected true shadow (nonshadow) pixels over that of total true shadow (nonshadow) pixels. The second type of accuracy is the user’s accuracy in terms of  $p_s$  and  $p_n$ , which are defined as

$$p_s = TP / (TP + FP)$$

$$p_n = TN / (TN + FN)$$

The parameter  $p_s$  ( $p_n$ ) denotes the ratio of the number of correctly detected true shadow (nonshadow) pixels over that of the total detected true shadow (nonshadow) pixels, and thus, the user’s accuracy can be used to measure the precision of the shadow detection algorithm. Combining the accuracies of the user and the producer, the third type of accuracy (overall accuracy)  $\tau$  defined as follows can be used to evaluate the correctness percentage of the algorithm:

$$\tau = (TP + TN) / (TP + TN + FP + FN)$$

Where  $TP + TN$  denote the number of correctly detected true shadow and nonshadow pixels;  $TP + TN + FP + FN$  is equal to the number of total pixels in the image.

Table 1  
 (Shadow Detection Accuracy Measurements for Figure 6(a))

Method	Producer’s accuracies		User’s accuracies		Overall accuracies
	$\eta_s$ (%)	$\eta_n$ (%)	$p_s$ (%)	$p_n$ (%)	$\tau$ (%)
Proposed	96.39	88.74	88.74	96.39	92.41
Tsai’s	94.63	65.27	65.27	91.63	76.24

Table 2  
 (Shadow Detection Accuracy Measurements for Figure 7(a))

Method	Producer’s accuracies		User’s accuracies		Overall accuracies
	$\eta_s$ (%)	$\eta_n$ (%)	$p_s$ (%)	$p_n$ (%)	$\tau$ (%)
Proposed	96.15	96.20	96.20	96.15	96.17
Tsai’s	95.64	90.86	90.86	95.64	93.19



## International Journal for Research in Applied Science & Engineering Technology (IJRASET)

Table 3  
 (Shadow Detection Accuracy Measurements for Figure 8(a))

Method	Producer's accuracies		User's accuracies		Overall accuracies
	$\eta_s$ (%)	$\eta_n$ (%)	ps (%)	pn (%)	$\tau$ (%)
Proposed	99.57	54.65	54.65	99.57	70.56
Tsai's	99.16	31.87	31.87	99.16	48.23

Table 4  
 (Shadow Detection Accuracy Measurements for Figure 9(a))

Method	Producer's accuracies		User's accuracies		Overall accuracies
	$\eta_s$ (%)	$\eta_n$ (%)	ps (%)	pn (%)	$\tau$ (%)
Proposed	96.89	84.56	84.56	96.89	90.30
Tsai's	93.44	89.46	89.46	93.44	91.40

Table 5  
 (Shadow Detection Accuracy Measurements for Figure 10(a))

Method	Producer's accuracies		User's accuracies		Overall accuracies
	$\eta_s$ (%)	$\eta_n$ (%)	ps (%)	pn (%)	$\tau$ (%)
Proposed	99.31	64.57	64.57	99.31	78.25
Tsai's	99.32	55.49	55.49	99.32	71.20

Table 6  
 (Average accuracies measurements for Table 1-5)

Method	Overall accuracies (Table 1)	Overall accuracies (Table 2)	Overall accuracies (Table 3)	Overall accuracies (Table 4)	Overall accuracies (Table 5)	Average accuracies
Proposed	92.41	96.17	70.56	90.30	78.25	85.53
Tsai's	76.24	93.19	48.23	91.40	71.20	76.05

## International Journal for Research in Applied Science & Engineering Technology (IJRASET)

From the aforementioned three types of accuracy, Table 1-5 show the accuracy comparison between Tsai's algorithm and our new algorithm for Figure 6(a)-10(a), respectively. Table 6 shown Average accuracies of our proposed and tsai's algorithm for Table 1-5 shown that accuracy of our new method is better than tsai's algorithm. Hence overall shadow detection using our new method gives better results than tsai's.

### VI. CONCLUSION

In this paper, our new analysis algorithm has been presented for detecting shadows of color aerial images. RGB color image transform into the gray image and then Otsu's method is used to determine a global threshold T for gray image to constructing the coarse-shadow map. Experimental results demonstrated that our new analysis algorithm has better shadow detection accuracy when compared with the Tsai's algorithm.

### REFERENCES

- [1] K.-L. Chung, Y.-R. Lin, and Y.-H. Huang "Efficient Shadow Detection of Color Aerial Images Based on Successive Thresholding Scheme," IEEE Transactions On Geoscience And Remote Sensing, Vol. 47, No. 2, February 2009.
- [2] V. J. D. Tsai, "A Comparative Study on Shadow Compensation of Color Aerial Images in Invariant Color Models," IEEE Transactions On Geoscience And Remote Sensing, Vol. 44, No. 6, June 2006.
- [3] L. Lorenzi, F. Melgani, and G. Mercier, "A Complete Processing Chain for Shadow Detection and Reconstruction in VHR Images," IEEE Transactions On Geoscience And Remote Sensing, Vol. 50, No. 9, September 2012.
- [4] H. Ma, Q. Qin, and X. Shen, "Shadow segmentation and compensation in high resolution satellite images," in Proc. IEEE IGARSS, Jul. 2008, vol. 2, pp. 1036-1039.
- [5] D. Cai, M. Li, Z. Bao, "Study on shadow detection method on high resolution remote sensing image based on HIS space transformation and NDVI index," in Proc. 18th Int. Conf. Geoinformat., Jun. 2010, pp. 1-4.
- [6] A. Makarau, R. Richter, R. Müller, and P. Reinartz "Adaptive Shadow Detection Using a Blackbody Radiator Model", IEEE Transactions On Geoscience And Remote Sensing, Vol. 49, No. 6, June 2011.
- [7] T. Kim, T. Javzandulam, and T.-Y. Lee, "Semiautomatic reconstruction of building height and footprints from single satellite images," in Proc. IGARSS, Jul. 2007, vol. 2, pp. 4737-4740.
- [8] W. Zhou, G. Huang, A. Troy, and M. L. Cadenasso, "Object-based land cover classification of shaded areas in high spatial resolution imagery of urban areas: A comparison study," Remote Sens. Env., vol. 113, no. 8, pp. 1769-1777, 2009.
- [9] A. M. Polidorio, F. C. Flores, N. N. Imai, A. M. G. Tommaselli, and C. Franco, "Automatic shadow segmentation in aerial color images," in Proc. XVI Brazilian Symp. Comput. Graph. Image Process., Oct. 12-15, 2003, pp. 270-277.
- [10] J. Huang, W. Xie, and L. Tang, "Detection of and compensation for shadows in colored urban aerial images," in proc. 5<sup>th</sup> World Congr. Intell. Control Autom. Hangzhou, China, Jun. 15-19, 2004, pp. 3098-3100.



10.22214/IJRASET



45.98



IMPACT FACTOR:  
7.129



IMPACT FACTOR:  
7.429



# INTERNATIONAL JOURNAL FOR RESEARCH

IN APPLIED SCIENCE & ENGINEERING TECHNOLOGY

Call : 08813907089  (24\*7 Support on Whatsapp)